Flash and Smash: Rapid Freezing of Muscle Fibers Activated by Photolysis of Caged ATP

Keiko Hirose, Thomas D. Lenart,* John M. Murray, Clara Franzini-Armstrong, and Yale E. Goldman‡
Department of Cell and Developmental Biology, *Biochemistry and Biophysics, ‡Physiology, and Pennsylvania Muscle Institute, University of Pennsylvania, Philadelphia, Pennsylvania 19104 USA

ABSTRACT A new approach was used to study transient structural states of cross-bridges during activation of muscle fibers. Rabbit skinned muscle fibers were rapidly and synchronously activated from the rigor state by photolysis of caged ATP in the presence of Ca^{2+}. At several different times during the switch from rigor to fully active tension development, the fibers were rapidly frozen on a liquid helium-cooled metal block, freeze-substituted, and examined in an electron microscope. The limits of structural preservation and resolution with this technique were analyzed.

We demonstrate that the resolution of our images is sufficient to draw the following conclusions about cross-bridge structure. Rigor cross-bridges point away from the Z-line and most of them are wider near the thin filaments than near the backbone of the thick filaments. In contrast, cross-bridges in actively contracting fibers stretch between the thick and thin filaments at a variable angle, and are uniformly thin. Diffraction patterns computed from contracting muscle show layer lines both at 38 and 43 nm indicating that active cross-bridges contribute mass to both the actin- and myosin-based helical periodicities. The images obtained from fibers frozen 20 ms after release of ATP show a mixture of rigor and active type cross-bridge configurations. There is little evidence of cross-bridges with the rigor shape by 50 ms, and the difference in configurations between 50 and 300 ms after photolysis is surprisingly subtle.

INTRODUCTION

Force development and shortening of muscle result from a cyclic interaction between myosin heads and actin filaments. A useful hypothesis about this interaction is that structural changes in cross-bridges (myosin heads attached to actin filaments) underlie mechanochemical transduction during the cross-bridge cycle (1, 2). The structure and disposition of cross-bridges in static states has been studied by x-ray diffraction and electron microscopy (EM). Longitudinal views of chemically fixed muscle in the rigor state (no ATP) show angled cross-bridges (1, 3–5). In insect muscle, the rigor cross-bridges are regularly arranged with a strong actin-filament-based periodicity (38.5 nm). The actin periodicity is present also in vertebrate, though weaker than in insect. This configuration is suggested to occur at the end of the power stroke (6) and is dictated by a fixed angle of interaction between myosin heads and actin monomers (7–11). Muscle fibers in other attached states, for example those in the presence of the nonhydrolyzable ATP analogue adenosine 5′-(β,γ-imino)triphosphate (AMP-PNP) show different configurations (12, 13). However, there is no direct evidence that these structural states occur in the physiologically relevant cross-bridge cycle.

Recently, the structure of cross-bridges in muscle fibers during steady-state contraction was preserved by rapid freezing and freeze-substitution, and conformational differences between rigor and active cross-bridges were detected by EM (14–16). Cross-bridges in active fibers show highly variable shapes and angles with an average angle of ~90° to the filament axis. Active cross-bridges maintain the myosin-based 14.3-nm periodicity. Some in vitro studies of isolated myosin heads bound to actin filaments in the presence of ATP also show variable angles (Refs. 17–20, but see Pollard et al. (21)).

However, interpreting these images is difficult because the active cross-bridges in these experiments are probably distributed among all of the states of the biochemical and mechanical cycles. Although each configuration of the cross-bridge may correspond to one specific state, the relationship between structural, biochemical, and mechanical states is not clear. In order to progress in establishing this correlation, structural studies are required in conditions where the populations of mechano-chemical states are either known or at least altered from the steady-state mixture.

Here we developed a new device that activates skinned muscle fibers by photolysis of caged ATP in the presence of Ca^{2+}, while monitoring tension, and then rapidly freezes the fibers at selected times after photolysis to trap the structural states in the transient condition. The initial biochemical and mechanical condition of the cross-bridges (rigor) is the most well understood and their structure is fairly homogeneous. The relationship between the mechanical condition and the biochemical state immediately after photolysis is thought to be relatively simple and partially synchronized (22). "Snapshot" images of the cross-bridges at several different time points during activation can be obtained by this approach. Some of the results have been briefly reported (23, 24).

MATERIALS AND METHODS

Experimental setup

The experimental setup is shown in Fig. 1. It is a "Cryo-Press" (Med-Vac, Inc., St. Louis, MO) modified to enable laser photolysis and tension meas-

Received for publication 28 December 1992 and in final form 17 March 1993.

0006-3495/93/07/397/12 $2.00

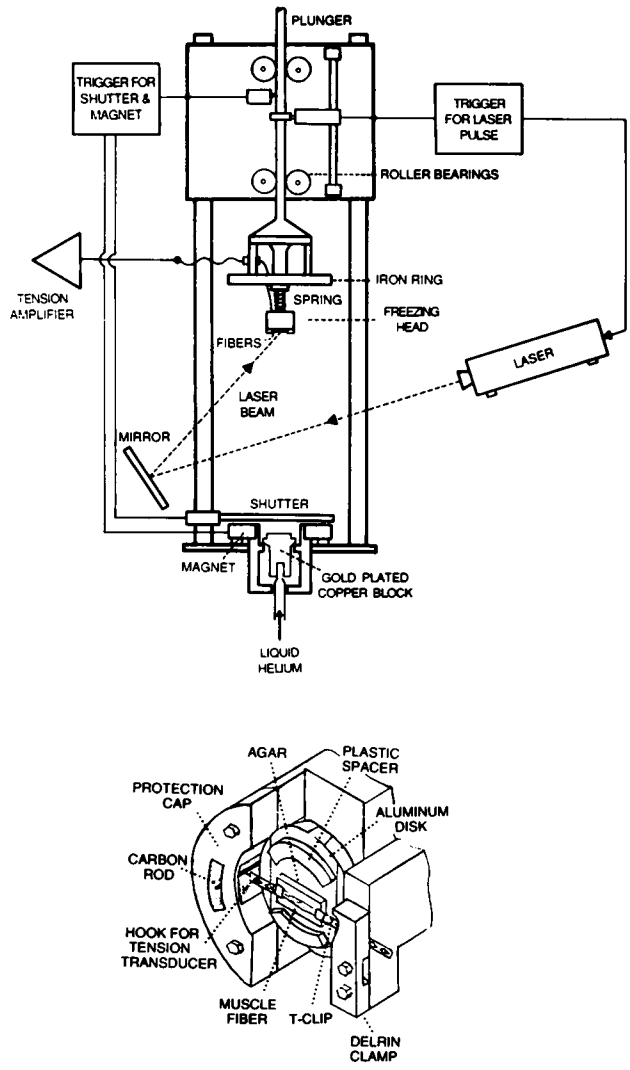

FIGURE 1 Top, a diagram of the freezing apparatus (modified from Cryopress, Med-Vac Inc. (25)). The freezing head falls onto a liquid-helium-cooled block of copper coated with gold. An optical sensor triggers a frequency-doubled ruby laser for photolysis of caged ATP at preselected time points (20, 50, 80, or 300 ms before freezing). The time interval between the laser pulse and freezing is adjusted by changing the positions of the optical sensor and the mirror. Bottom, a more detailed diagram of the freezing head. Small bundles of one to five skinned fibers are wrapped with T-clips at both ends, and mounted between a hook connected to the tension gauge (Akers 801, protected from excessive deflections (26)) and a clamp on the freezing head.

urement. Samples were mounted on a freezing head attached to a plunger. The head was released to descend by gravity, and the sample was slammed onto a metal block cooled with liquid helium. The head was modified to incorporate attachment for the muscle fibers and a tension transducer. This allows us to monitor the tension up to the time of freezing. A semiconductor strain gauge (Akers AE801) was extended by a thin carbon rod. A steel hook was attached to the carbon rod 2.5 mm from the end of the strain gauge. The transducer housing provided mechanical limitation to the motion of the strain gauge to protect it from breakage during the freezing event. The metal block was ultrapure copper polished to a mirror finish and plated with gold. In order to provide clearance for the transducer protection cap and fixed mounting clamp, the diameter of the top part of the block was reduced to 10 mm. A specimen mount was made from an appropriately trimmed, easily removable aluminum disk (25, 26). Two plastic spacers (0.5-mm thick) and a block of 2.5% agar (0.5- to 0.75-mm thick, 5 mm long) were glued with cyanoacrylate ester to the disk. The agar served as a cushion behind the fiber. A thin smear of vacuum grease around the free edges of the disk prevented solution leakage. Segments of muscle fibers equal in length to the agar cushion were wrapped with T-clips at both ends (27). The T-clips were made with long tails that fit into the delrin-fixed clamp at one end and over the force transducer hook at the other end of the freezing head.

An auxiliary device was made to exchange solutions. Several small, shallow wells (diameter, ~8 mm) made of Teflon were embedded in an aluminum plate. Each well had a magnetic stirrer. The freezing head with a sample was attached to a bridge above the well with the sample side down. The head was gently lowered so that the sample was immersed in the solution. The surface of the solution (~100 μl/well) was higher than the edge of the well. In this way only the muscle fibers were immersed in a solution and the other parts (e.g., transducer) were kept dry.

A frequency-doubled ruby laser was used to produce the laser pulse for photolysis (30 ns, at 347 nm) (28). Aiming of the laser beam was done by changing the position and orientation of the mirror. The time for descent of the head was ~200 ms. Thus, for time intervals shorter than ~200 ms, caged ATP was photolyzed while samples were dropping toward the metal block. During the fall, a flag attached to the plunger passed through an optical sensor and thus triggered the laser pulse. Timing of the trigger was controlled by changing the height of the optical sensor. For the longer time points a digital pulse generator delivered the timing pulses that triggered the laser prior to the fall of the freezing head. In a series of 20 trials with the same settings the time interval between the laser pulse and the freezing varied by no more than 2.5 ms for a 250-ms time interval and 0.5 ms for a 20-ms interval.

Preparation of muscle fibers

Fiber bundles from rabbit psoas muscle were skinned in relaxing solution (104 mM potassium propionate, 5 mM $MgCl_2$, 10 mM EGTA, 20 mM 1,4-piperazinediethanesulfonic acid (PIPES), 4.6 mM ATP, 0.1 mM phenylmethylsulfonyl fluoride, pH 6.9) plus 0.5% Triton X-100 at 4°C for 1–2 h, rinsed with the same solution without Triton X-100, transferred to 50% glycerol either in relaxing solution or in rigor solution (same as relaxing solution but without ATP), and kept at −20°C up to 1–2 days.

Single fibers or groups of two to five fibers, ~5 mm long, were dissected from the skinned bundles under silicone oil, attached to T-clips, and mounted on the freezing head. They were sequentially put into rigor solution without glycerol, into rigor solution containing calcium (1.2 mM $MgCl_2$, 20 mM calcium EGTA, 33 mM 1,6-diaminohexane-*N,N,N′N′*-tetraacetic acid (HDTA), 100 mM *N*-tris(hydroxymethyl)methyl-2-aminoethanesulfonic acid (TES), 10 mM glutathione, pH 7.1), and finally in the same solution plus 10 mM caged ATP. Excess solution was removed by aspiration, and then the fibers were frozen at a preselected time after photolysis of caged ATP. We chose to examine four time points after photolysis, 20, 50, 80, and 300 ms. The range of times measured on actual traces were 18–25, 40–50, 75–85, 280–290 ms. After freezing, the head was quickly transferred into liquid nitrogen, and the T-clips were cut using scissors. The aluminum disk with frozen sample was detached from the head and stored in liquid nitrogen.

Electron microscopy

The samples were freeze-substituted with 2% OsO_4 in acetone at −80°C for 2 days, warmed to −20°C, transferred to fresh OsO_4/acetone and kept for ~2 h. They were then warmed to room temperature and rinsed with acetone. The agar block with the muscle fiber was detached from the aluminum disk. The samples were stained *en block* with 1% uranyl acetate in acetone at room temperature and embedded in araldite. Sections were cut tangent to the frozen surface, with the direction of cutting being perpendicular to the filament axis. They were stained with potassium permanganate and lead citrate and examined in a Philips EM410 electron microscope. Images showing no ice damage were used for analysis.

Image analysis

Selected regions of the micrographs were digitized using a scanning flatbed microdensitometer (Perkin-Elmer 1010G) with a step size of 50 μl for im-

ages taken at a magnification of 44,400 or 25 μl for images at magnifications from 17,700 to 33,900. Fourier transforms, filtered images, and modeled images were calculated using the Semper image processing system (Synoptics Ltd.) on a Sun4/330 computer.

The position of the meridional reflection at ~14 nm in the diffraction patterns was taken as 14.3 nm, and all other spacings were scaled relative to 14.3 nm. The images were also rotated to set the equator of the Fourier transform horizontal and made orthogonal by lateral shearing to set the meridian (as defined by the maximum intensity of the ~14-nm meridional spot) vertical. Power spectra of the Fourier transforms from the corrected images were then added together to enhance the diffraction spots relative to background.

Catalase crystals

Catalase crystals were used to investigate the resolution capabilities of our freeze-substitution technique. Tiny droplets of a slurry of bovine liver catalase crystals (Sigma Chemical Co., St. Louis, MO) were rapidly frozen by immersing them in a liquid propane/isopentane mixture (29), freeze-substituted and embedded, sectioned and examined as described above. Lattice distortions in these images were corrected by a standard "unbending" procedure (30). Briefly, a reference unit cell was cross-correlated with the image to be "unbent." The peaks in the resultant cross-correlation map were indexed, thereby defining their locations in an ideal lattice. The actual and ideal locations of this set of lattice points were used to construct a two-dimensional warping function. This function guided the interpolation necessary to remove the geometric distortion of the original image.

Modeling of cross-bridges

In order to test the effects of the limited resolution and background density fluctuations on visibility of cross-bridges, we produced model images of stylized cross-bridges and treated them to mimic real EMs. The original model was blurred by multiplying the Fourier transform of the image by a circular Gaussian filter function with a value of 1.0 at the origin and 0.2 at radius corresponding to 7 and 10 nm for the model images at 7- and 10-nm resolution. This blurring is intended to simulate the loss of fine detail caused by our freeze-substitution, embedding, sectioning, and EM imaging procedures. To these blurred model images we added noise to simulate the effects of variable staining, film granularity, and other random density fluctuations. The spectral distribution of this added noise was taken directly from our EM images by the following procedure. Periodic densities in the Fourier transform from a typical EM were masked. After randomizing the phase, the inverse transform was calculated to create "noise." The blurred model images with noise added were then filtered by multiplying the Fourier transform by a low-pass filter function that has a value 1.0 out to an appropriate radius and then falls as a Gaussian decay.

RESULTS

Structural preservation and resolution

In order to study the configuration of cross-bridges in various functional states, we must insure sufficient resolution and good preservation of the structure of the sarcomere. The spatial resolution of an EM image of a freeze-substituted, embedded, and sectioned protein array was estimated using a slurry of catalase crystals frozen in a liquid propane/isopentane mixture and processed using the same methods as the muscle fibers. Images of regions of the sections that happened to be oriented appropriately (*i.e.*, showing clear lattice lines in two directions) were digitized, unbent as described under the Materials and Methods section, and the Fourier transform (FT) was calculated. We display as two-dimensional density plots the results of the FT calculation as gray scale plots of the power spectrum (magnitude squared) of the FT as a function of spatial frequency. These computed power spectra are termed "diffraction patterns," by analogy

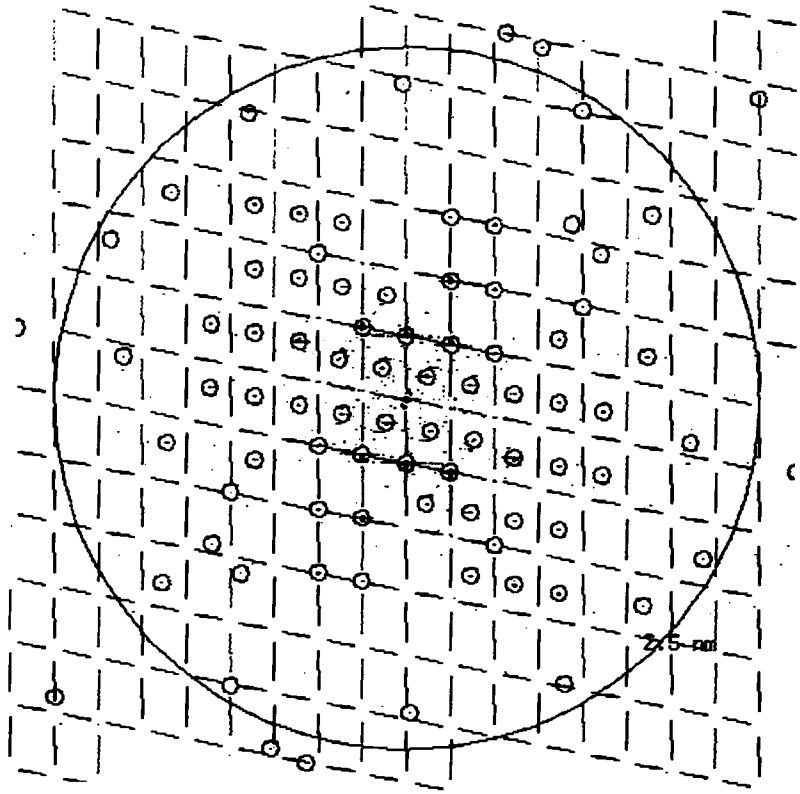

FIGURE 2 The diffraction pattern computed from a thin section of freeze-substituted and embedded catalase crystals. The diffraction pattern was calculated from a digitized and unbent EM image, and displayed as the ratio of pixel amplitude to local mean amplitude. The peaks significantly above background are marked by small circles. The sample was a slurry of small crystals in random orientations. The chosen image apparently included a superposition of more than one crystallite, since at least two different lattices were observed, one of which is marked by the dashed line. The large circle indicates a reciprocal spacing of 2.5 nm. The peaks on the lattice points demonstrate that the apparent resolution of the image is about 2.6 nm.

to the usual presentation of x-ray diffraction analysis. The diffraction pattern from a digitized and unbent EM image is shown in Fig. 2. The significant peaks in the spectrum are marked with small circles. At least two different lattices were present in the selected region, one of which is marked by the grid. The large circle indicates a resolution of 2.5 nm. Lattice reflections out to ~2.6 nm are present in the power spectrum indicating the resolution of the periodic parts of the image is better than 3 nm. Power spectra of images before unbending showed significant lattice reflections to ~3.6 nm. The relationship of these results on freeze-substituted catalase crystals to interpretation of the muscle fiber images is treated under the Discussion section.

Fibers frozen at short and long intervals after activation show well-maintained lateral order of the sarcomere structure and regular cross periodicities (Fig. 3). The M-lines and Z-lines are nearly perpendicular to the filament axis. In active fibers the lateral alignment is typically better with the photolysis technique than we have been able to achieve when using activation by solution exchange. The computed diffraction patterns from images of rigor and active fibers show many clear features, but the resolution apparent from the diffraction patterns was not as high as from the catalase crystals. Since contribution from nonperiodic features in the images would mask true periodicities in the diffraction patterns, we summed diffraction patterns from several regions to improve the signal-to-noise ratio. For this analysis, the images were scaled and rotated to align them as described under the Materials and Methods section. The averaged diffraction pattern for a set of fibers at 50 ms (Fig. 4 *a*) shows a number of meridional and layer line reflections in the region from 43 nm out to 7.2 nm. Fig. 4 *b* shows a plot of the summed intensity within a vertical band corresponding to ~6 nm on either side of the meridian using fibers in rigor and at 50 and 80 ms. Several myosin-based peaks (43, 22, 14, 7.2 nm) and actin-based peaks (36, 19, 5.9 nm) are clearly evident in the logarithmic plot of this summation. These results indicate that the periodic structures in the fibers are preserved at least to 6–7-nm resolution. Throughout the paper, the first actin layer line is denoted by a definite value (36 or 38 nm), where it could be precisely determined, or by an intermediate value (~37 nm) where it could not be measured accurately enough to distinguish between 36 and 38 nm.

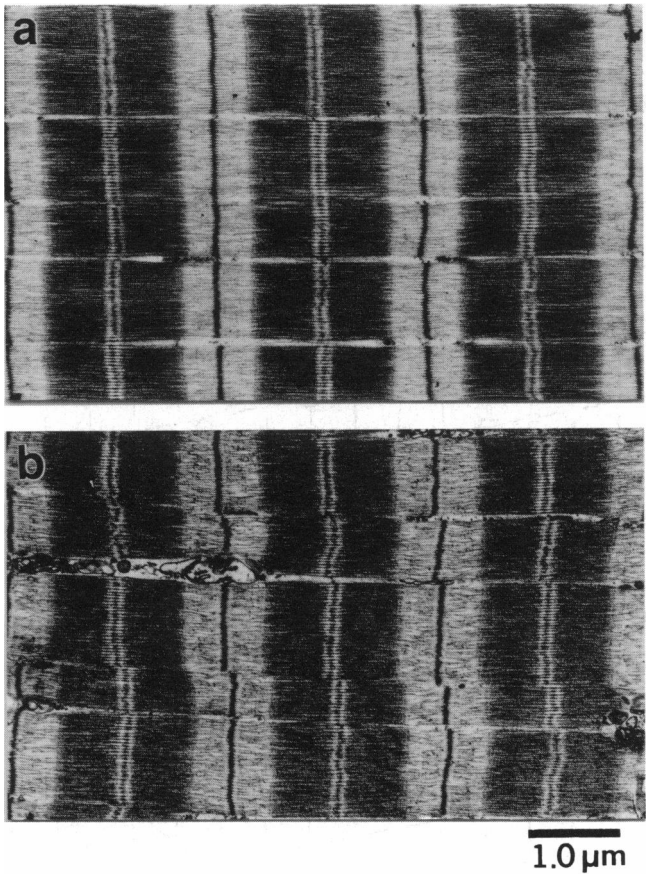

FIGURE 3 Low magnification images of muscle fibers frozen at 50 ms (*a*) and at 300 ms (*b*) after photolysis of caged ATP, showing that the striations remain well aligned during activation.

Structural changes following activation

EM images of muscle fibers in the transient structural states during activation from the rigor state were obtained by ultrarapid freezing following laser photolysis of caged ATP. Tension shows a transient dip in the first 20 ms after photolysis indicating cross-bridge detachment and reattachment, followed by an increase to a plateau at approximately 100 ms.

Images of longitudinal sections 40–70-nm thick show clear structural differences between fibers frozen in rigor (Fig. 5 *a*) and 80 ms after activation by photolysis of caged ATP (Fig. 5 *b*). The structure of rigor muscle is relatively regular (Fig. 5 *a*); periodic striations (average spacing, 36 nm) perpendicular to the filament axis are seen, suggesting regular arrangement of cross-bridges. A 36-nm periodicity is not visually apparent in images of active fibers (Fig. 5 *b*). Finer striations are seen in some regions, but only very locally. Overall the disposition of the cross-bridges is less ordered.

The computed, averaged diffraction pattern from rigor fibers (Fig. 6 *a*) shows a strong and rather broad layer line with a peak position at a spacing of 36 nm. This spacing corresponds to the periodicity of the lateral striations observed in the overlap region of images of rigor fibers (Fig. 5 *a*). It is thought to arise from cross-bridges bound regularly along thin filaments having a helical structure with a half-pitch of 36 nm. The thick-filament-derived 43-nm layer line is visible but weak (Fig. 6, *a* and *c*).

In the diffraction pattern from the fibers frozen 80 ms after photolysis (Fig. 6 *b*), layer lines at 38 and 43 nm are both clearly visible, and their intensities are similar (Fig. 6, *b* and *d*). These two layer lines are resolved only when 10 or more diffraction patterns are averaged. The peak intensity along the 38 nm layer line is closer to the meridian than that of the 36 nm layer line in rigor. The plots of intensities integrated in the direction parallel to the equator (Fig. 6, *c* and *d*) indicate the existence of several additional reflections, which are weakly seen in the two-dimensional patterns. Peaks with

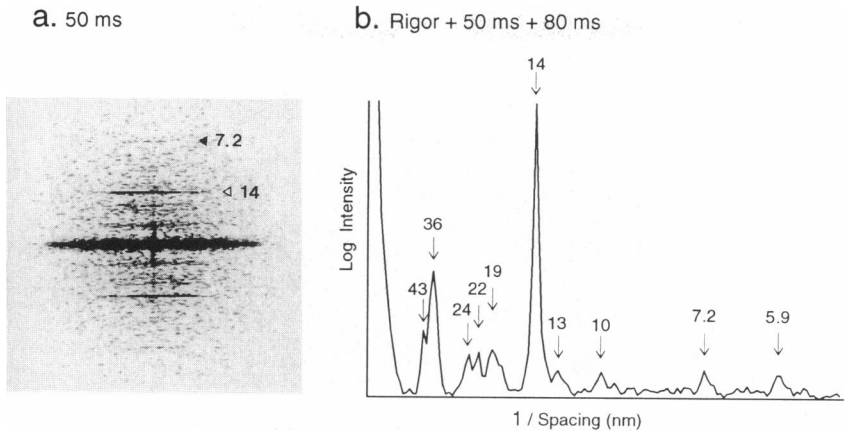

FIGURE 4 (*a*) An averaged diffraction pattern computed from digitized images of the fibers frozen at 50 ms after the photolysis laser pulse. Eight selected diffraction patterns from the overlap regions were used to calculate the average. The myosin-derived meridional layer line with a spacing of 7.2 nm is visible. (*b*) A graph showing density distribution of a computed, averaged diffraction pattern. An average of 82 different diffraction patterns from the overlap regions of the fibers frozen in rigor, and at 50 and 80 ms after activation was used. The intensities in the region within ~1/6 nm^{-1} of the meridian were added together in the direction parallel to the equator, as if the intensity within a narrow slit parallel to the equator was summed. The background (approximated by a series of linear segments) was subtracted from the logarithm of integrated intensity. The result is plotted against spatial frequency in the meridional direction. Spacings of the significant peaks were calculated assuming the strongest myosin reflection to be 14.3 nm. The approximate distances in real space are indicated. A peak at 5.9 nm is evident.

spacings that are harmonics of 43 nm (22 nm), and of 36–38 nm (18–19 and 13 nm) are seen both in rigor and at 80 ms, but more clearly in the latter. The plot from rigor muscle has a fairly strong peak at 24 nm.

EM images of thinner longitudinal sections (~30 nm) in the (1,1) planes of rigor fibers are dominated by angled cross-bridges giving the appearance of arrowheads pointed toward the M-line (Fig. 7 *a*). Profiles of cross-bridges lying in the plane of the section are visualized. Most cross-bridges have a triangular shape, with the base near the thin filament and apex near the thick filament shaft (Fig. 7 *a*, black and white arrowheads). We refer to cross-bridges with a triangular shape and angled orientation as the "rigor configuration." There is a fair degree of order; fine periodicities can be seen across the A-band, although they are more difficult to see in this thin section than in the thicker sections as shown in Fig. 5. Periodic beading (increased width or density) of the thin filament is visible due to cross-bridges arising from the out of plane thick filaments. The computed diffraction pattern clearly shows the 14.3-nm myosin layer line, and the ~37-nm actin layer line. The structure of fibers frozen in rigor solution plus caged ATP but without photolysis is similar to standard rigor.

At 20 ms after photolysis the tension is just beginning to rise following the initial decrease. Extensive cross-bridge attachment is observed in the EMs in most regions of the overlap zone (Fig. 7 *b*), but the average cross-bridge angle is different from that in rigor, so that the arrowhead appearance is lost. Some cross-bridges point toward the M-line, but others are at approximately right angles to the thin filaments or point toward the Z-line. The fine periodicities across the A-band are visible over very short distances. Some cross-bridges are triangular as in rigor, but most are thinner and have more uniform thickness in the interfilament space. Although weaker than in rigor, both the myosin 14.3-nm and actin ~37-nm layer lines are present in the computed diffraction pattern. Overall there is less appearance of order than in rigor due to more variation in cross-bridge dispositions in different areas and less regular beading of the thin filaments. Some regions have few attached cross-bridges.

At 50 ms after photolysis, the tension has risen to approximately half of the maximum isometric tension, at 80 ms it is at 70–90% of maximum, and at 300 ms it has reached the plateau. At 50 ms the angle of the cross-bridges is variable, but the average angle is approximately perpendicular to the filament axis (Fig. 7 *c*). In some regions a 14.3-nm axial periodicity predominates near both myosin and actin filaments (15). Cross-bridges with triangular shape are rare, and most of the cross-bridges are thinner than in rigor. With respect to those cross-bridges at 20 ms that are not in the rigor configuration, there is no obvious difference in appearance between 50 and 20 ms. In the computed diffraction pattern at 50 ms, the 14.3-nm reflection is visible. At 80 (not shown) and 300 ms (Fig. 7 *d*), both the image and diffraction pattern are similar to those at 50 ms.

Averaged diffraction patterns from 20–40 images from fibers at 50 ms (data not shown) clearly show lines at 38 and 43 nm, such as illustrated in Fig. 6, *a* and *d*, for fibers at 80 ms. Patterns from a single image however are too noisy to resolve the two lines. At 20 and 300 ms we did not have as much data so we did not obtain average patterns.

DISCUSSION

Flash and smash method

By combining photolysis of caged ATP and rapid freezing we captured transient structural states of cross-bridges in muscle fibers after activation and correlated these states with force production of the fibers. The tension measured on the freez-

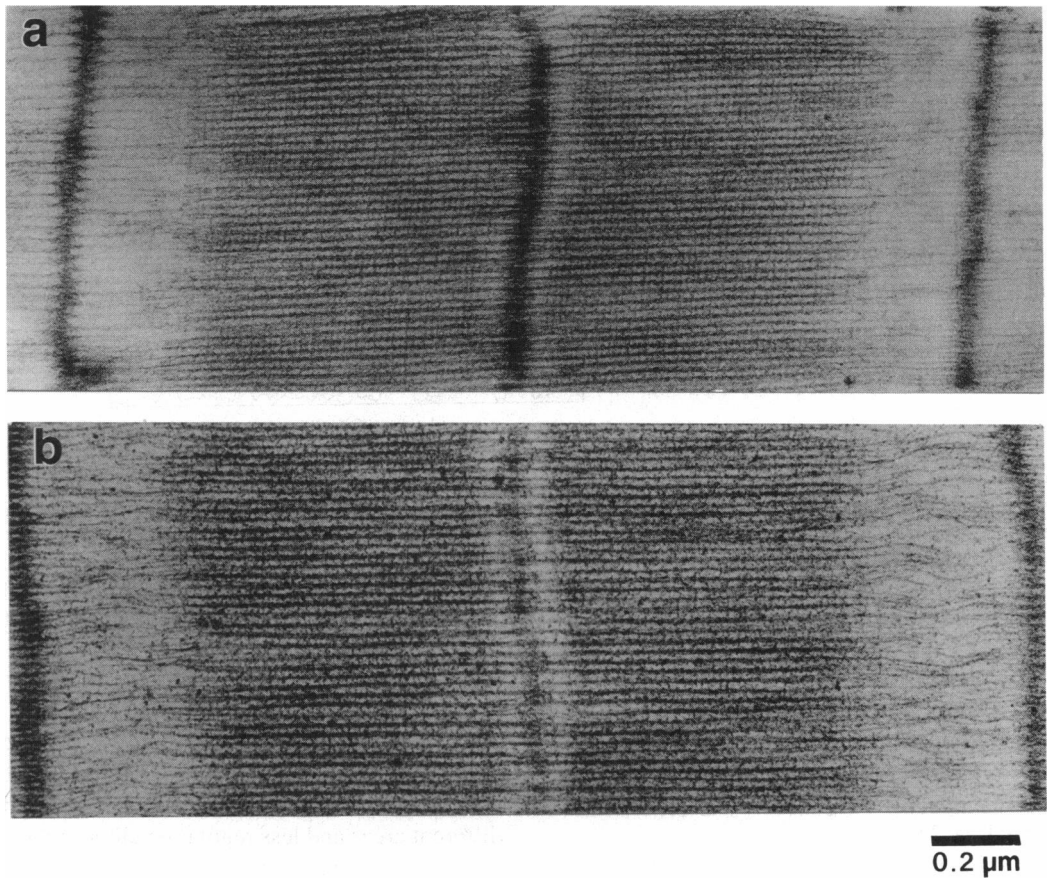

FIGURE 5 Micrographs of longitudinal sections of a fiber in the rigor state (*a*) and a fiber frozen 80 ms after activation by caged ATP photolysis (*b*). The M-lines are in the center of the micrographs. Fine striations perpendicular to the filament axis are seen in the overlap regions, especially in the rigor fiber, indicating some regularity in the disposition of cross-bridges. The appearance of the overlap region in the active fiber is more disordered than in the rigor fiber.

ing head until impact was similar to that observed previously (22). The minimum time interval between activation and freezing (~15 ms) and the time required for freezing (<1 ms) are short compared to the cycle time for the cross-bridge ATPase in muscle fibers (300 ms (31)). The approach has several major advantages over the use of steady state contractions: 1) transitional states during activation of the cross-bridges can be studied; 2) the sarcomere structure obtained is much more orderly (Fig. 2), probably because activation of the fibers is uniform and the time interval between activation and freezing is short.

Several structural studies on muscle fibers have used photolysis of caged ATP to partially synchronize cross-bridges as they are rapidly activated from the well-defined rigor state. Electron paramagnetic resonance (32, 33) and fluorescence spectroscopy (34) following photolysis of caged ATP within rigor muscle fibers have indicated a rapid disordering of the cross-bridge array before the main force development. X-ray diffraction (35) showed a rapid decrease in the ratio of equatorial reflections I_{11}/I_{10} preceding tension development and a slower increase in the 14.3-nm reflection. Our approach using electron microscopy allows observation of individual molecules in the images, and also permits measurement of average periodic spacings and relative mass distribution from the computed transforms.

Preservation and resolution

A crucial point for interpretation of the present electron micrographs is the degree of preservation of the native ultrastructure and the resolution at which the structure can be detected. Freeze-substitution is known to give excellent preservation of cytoplasmic structures (36, 37). Our freeze-substituted catalase crystals and rabbit muscle fibers showed resolution of periodicities smaller than 3 and 6–7 nm, respectively. Freeze-substitution of muscles intrinsically more ordered than rabbit showed reflections at 6–7 nm (frog muscle (38, 39)), and ~6 nm (insect muscle (M. K. Reedy, Duke University, personal communication)).

These two values (<3 nm in catalase, 6–7 nm in muscle) obviously cannot be equated directly because the protein crystal has considerably more order than a muscle fiber. Contacts between the protein molecules in the crystal retain the individual subunits on a regular lattice and at precise orientations. Thus *periodic* diffraction spots due to the regular arrangement of the molecules on a lattice are much more

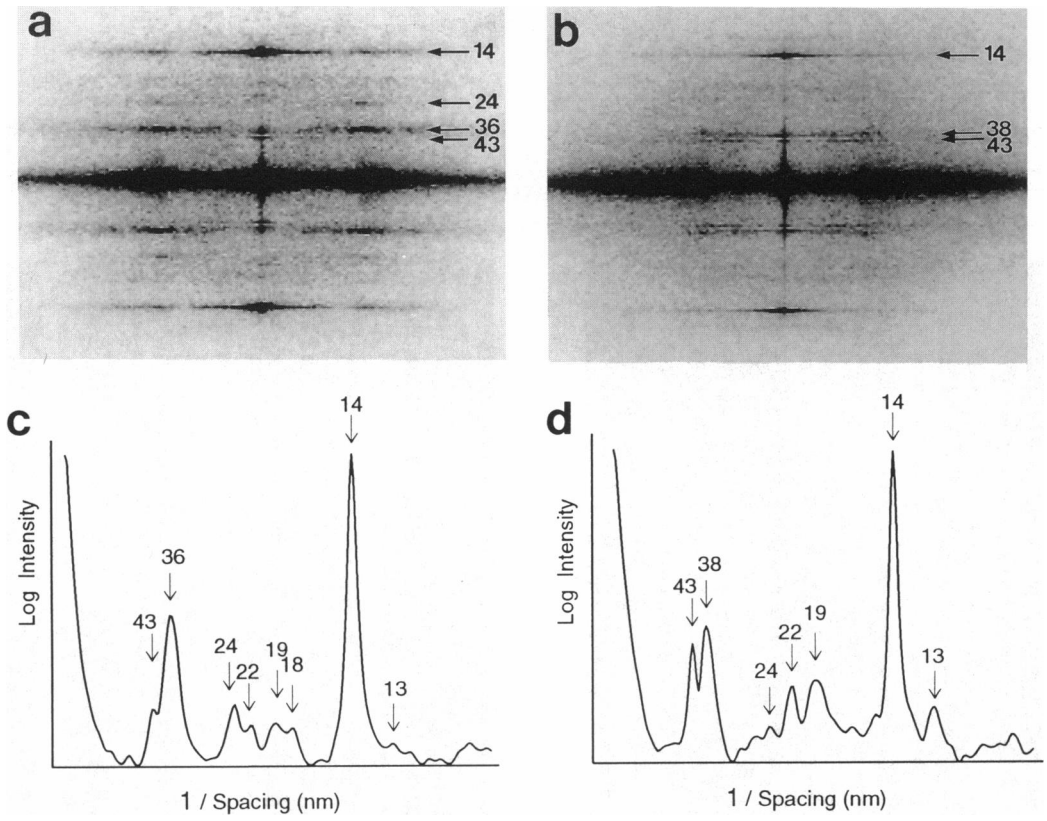

FIGURE 6 Computed, averaged diffraction patterns from 37 selected areas of overlap regions from A-bands in the rigor state (*a*) and 39 selected areas of overlap regions at 80 ms (*b*). *c* and *d* are logarithmic plots of summed intensities in *a* and *b*, integrated in the direction parallel to the equator as in Fig. 4. The diffraction pattern from rigor fibers has a strong, rather broad layer line at a spacing of 36 nm, whereas the pattern from active fibers shows two sharp layer lines at 43 and 38 nm. The 14.3-nm myosin meridional reflection is strong in both cases. In rigor, a layer line at 24 nm is fairly strong. This layer line is not clear in the pattern from active fibers.

intense in the crystal than in a muscle. On the other hand, if we consider the basic similarity in amino acid backbone and side groups away from the crystal contacts, there is no reason to expect major differences between catalase and muscle proteins with respect to distortion introduced by processing. Thus small features, such as edges of the protein subunits that result in the observed image contrast are likely to be preserved to a similar extent in the two types of specimen.

The apparent resolution estimated from the *periodic* densities in the diffraction patterns is worse than the true resolution due to factors such as low long-range order of the native structure, artifactual distortion, noise in the images, or true physiological variability of the disposition of the proteins. That some periodic features of the images are obscured by random diffuse intensity variations induced by the above factors is indicated by the increased relative intensity of periodic densities in averaged compared to nonaveraged diffraction patterns. In muscle fibers, although periodic register in the cross-bridge arrangement is observed as striations perpendicular to the filament axis, the register is not accurately maintained over the entire image (Figs. 5 and 7). Thus, it would be more difficult to see the higher order reflections in the diffraction patterns from muscle fibers than in the patterns from a crystal, even if small details were equally well preserved in the two samples. The intensities at spacings smaller than 14.3 nm were usually weak in the diffraction patterns from single half sarcomeres in thin sections of muscle fibers. In this case, an important limiting factor is probably the intrinsic long range disorder and structural variations in the original structure, rather than a lack of preservation of small details by the freeze-substitution technique.

We observed that the cross-bridges in the images obtained following photolysis of caged ATP were very different from those in rigor, with considerable variation in the shape and angle. A crucial issue in interpreting these observations of micrographs with limited resolution and noise is the extent to which the observed variations are indicative of real structural differences between cross-bridges in the muscle fibers. We have examined this issue using model images to test the reliability of detecting changes in the shape and orientation of the cross-bridges. The major shape variation is a profile that is either uniform across the interfilament space or triangular, with a broad base next to the thin filament (5, 15, 16, 40). Differences in orientation appear as variations in the direction and degree of tilt of the cross-bridges relative to the filament axis.

EMs were simulated by creating a model of cross-bridges, and then by blurring and adding "noise" created from intensity variations in the actual micrographs. The "noise" contains fluctuations derived from nonperiodic real structures in

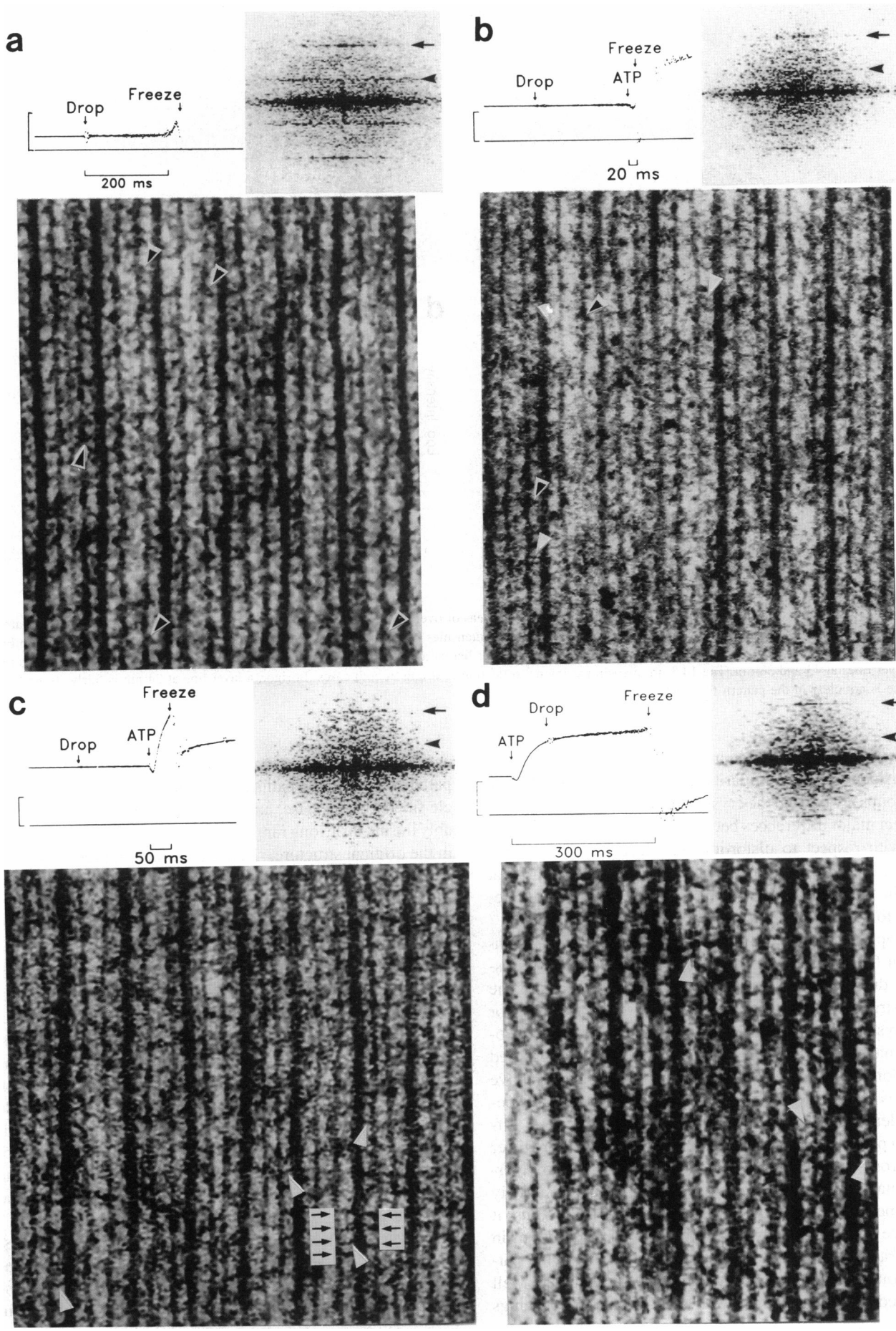
a
Drop
Freeze
200 ms
b
Freeze
Drop
ATP
20 ms
c
Freeze
Drop
ATP
50 ms
d
Drop
Freeze
ATP
300 ms

the muscle as well as resulting from specimen preparation and the imaging process (see Materials and Methods). Fig. 8, *e–l*, shows models of cross-bridge densities with either uniform width or a triangular shape and with angles of 65°, 79°, or 95° relative to the filament axis. With these angles, the axial positions of the distal end of the cross-bridges at the center of the thin filament are shifted by 8, 3, and −1 nm toward the M-line from their origin on the thick filament surface. The axial displacement in these model densities is similar to that previously used in a model that explains changes in the 14.3-nm meridional x-ray reflection during force generation (41). The original model (Fig. 8 *e*) was blurred to give a resolution either slightly worse (20% contrast at 7 nm, Fig. 8 *g*) or much worse (20% contrast at 10 nm, Fig. 8 *j*) than the estimated lowest resolution of our images. The blurring is intended to simulate the loss of fine detail caused by the freeze-substitution, embedding, sectioning, and EM-imaging procedures. To the blurred model images we added "noise" to simulate the effect of variable staining and other random density fluctuations as described under the Materials and Methods section. The "noise" used is an estimation of the real noise due to specimen preparation and imaging process, but also contains some density fluctuations derived from nonperiodic real structures in the muscle. Because nonperiodic, but real structural variation (e. g., cross-bridges with variable angles) contributes to the diffuse intensity in the power spectrum of our real images, the "noise" added to the model images overestimates the actual true noise. After blurring and noise addition, the model images (Fig. 8, *h* and *k*) are very similar to our unprocessed micrograph (Fig. 8, *a* and *b*). Recognition of cross-bridge shapes and angles is made easier by low-pass filtering that removes the very small-scale density fluctuations or random speckle smaller than the significant structural features. The results of applying the same low-pass filter to an original micrographs and to the noisy blurred model data is shown in Fig. 8, *c* and *d*, and Fig. 8, *i* and *l*.

Careful examination of the images permits one to classify reliably different individual cross-bridges as to shape and angle. The five authors of this paper tested visual discrimination of 120 blurred noisy model sites at 7- and 10-nm resolution (Fig. 8, *i* and *l*) containing either a cross-bridge or no cross-bridge. At 7-nm resolution, a mistake in recognizing a missing cross-bridge was made in 3 ± 3% of the cases, a mistake in assigning the right shape was made in 8 ± 3% of the cases, a 30° error in angle assignment was made in 4 ± 4%, and a 15° error in 27 ± 4% of the cases. At 10-nm resolution the errors were 6 ± 2, 14 ± 4, 8 ± 3, and 31 ± 5%. These results show that, despite the limited resolution of our micrographs, we can expect to resolve some shape differences (triangular versus uniformly thin) and an angular difference of ~30°. A 15° difference in angle is detected less reliably, but still quite well at 7-nm resolution.

Structure of active and rigor cross-bridges

Cross-bridges in the fibers during steady contraction have previously been reported to differ from rigor cross-bridges with respect to their periodicities, angles, and shapes (14–16). Our images and diffraction patterns from the fibers activated by caged ATP photolysis also show clear differences from the rigor fibers. Averaging of the diffraction patterns revealed additional features. Two layer lines were observed in the region near 40 nm, one with a 43-nm periodicity derived from thick filaments and another with a 38-nm thin-filament-derived periodicity (see also Ref. 14). Both of these layer lines were also observed in rapidly frozen frog fibers activated from the relaxed state by photolysis of caged Ca^{2+} (39, 42). The diffraction pattern from the rigor fibers showed a layer line at 24 nm, which was previously observed in x-ray diffraction studies (43, 44). The origin of this layer line in rigor muscle is an interaction between thin and thick filament periodicities as described earlier (45).

The changes that we observed in our images are consistent with those previously observed in in vitro studies. Three-dimensional reconstructions of isolated filaments (9–11) show that myosin heads bound to actin filaments in rigor have a fixed attachment angle, producing the characteristic arrowhead appearance. When myosin heads are trapped on isolated actin filaments in the presence of ATP by either negative staining or rapid freezing, they have variable configurations, which are different from rigor (Refs. 17–20, but see

FIGURE 7 Digitized and filtered images of longitudinal thin sections, their computed diffraction patterns and tension records of muscle fibers frozen in the rigor solution plus caged ATP without photolysis (*a*), and at 20, 50, and 300 ms after photolysis (*b*, *c*, and *d*, respectively). In the tension records, "Drop" indicates the time at which the freezing head starts falling. Caged ATP is photolyzed by the laser pulse at the arrow "ATP," and the fibers are frozen at the arrow "Freeze." The traces become noisy at the moment of impact. The apparent tension rise in *a* just before freezing is an artifact due to a current induced in the leads of the tension transducer by the strong magnet of the freezing chamber. This artifact was eliminated in later experiments. At 20 ms, tension is beginning to rise following a brief initial decline; at 50-ms tension is about half of the maximum level; and at 300-ms maximum isometric tension has been reached. The vertical bars in the tension records represent 0.5 mN in *a* and *d*, 1 mN in *b* and *c*. Experiments were conducted at room temperature (~20°C). Sections are parallel to the (1,1) planes and contain a single layer of filaments, alternating between one thick and two thin filaments. The M-lines are toward the top of the figure. For purposes of display, noise in the images was reduced using a median or local mean filter with a small kernel. In rigor (*a*), the arrowhead appearance of the cross-bridges can be seen clearly by sighting along the filaments toward the M-line. Fine periodicities that can be seen by glancing across the myofibril are probably a combination of the ~37-nm actin period labeled by cross-bridges and the 14.3-nm myosin period. At 20, 50, and 300 ms, the arrowhead appearance is lost and cross-bridge disposition is more disordered. Black and white arrowheads show examples of triangular-shaped cross-bridges, which are common in rigor but rare at 50 and 300 ms. White arrowheads show cross-bridges having uniform width, which predominate at 50 and 300 ms. The groups of equally spaced arrows in *c* indicate the 14.3-nm periodicity. The diffraction pattern was computed from the region shown. The magnification of the images was calibrated assuming that the third order myosin layer line in the Fourier transform occurs at 14.3 nm (*black arrows*). Black arrowheads indicate a spacing of 37 nm. During activation the layer line in this region is slightly shifted toward the equator from the position of the arrowhead.

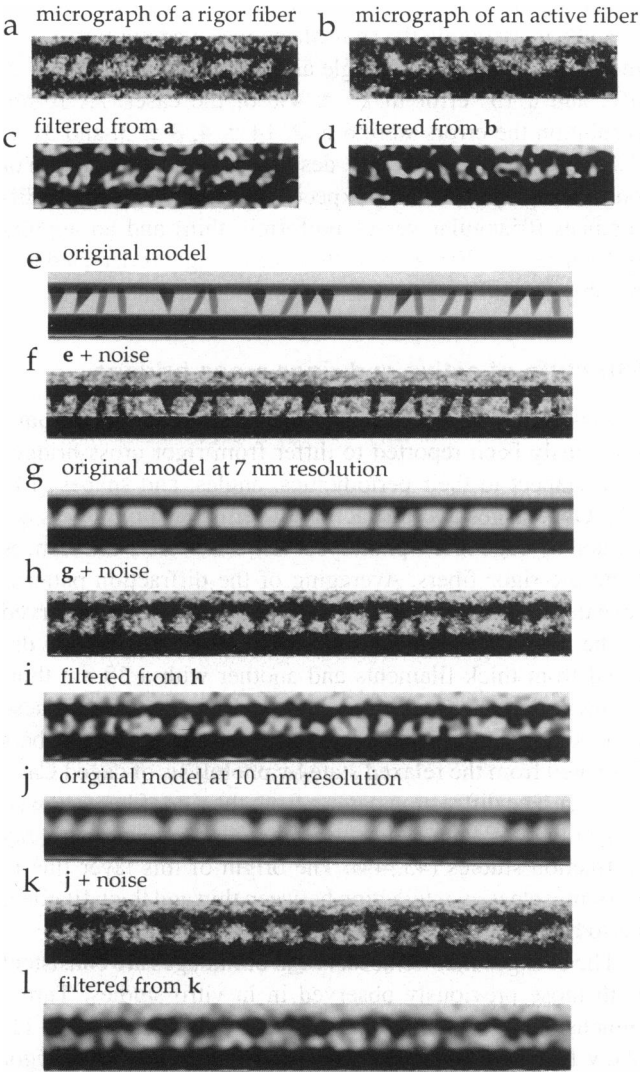

FIGURE 8 Micrographs (*a–d*) and computer-calculated models (*e—l*) that show various cross-bridges. The M-line is toward the right side of the figure. *a* and *b* are small portions of the micrographs of a rigor fiber and an active fiber, respectively (raw data). *c* and *d* are the low-pass filtered images from *a* and *b*, respectively. These filtered images were calculated by weighting the Fourier transform from the original image by a low-pass filter function that has value 1.0 out to a resolution of 5.7 nm, then falls as a Gaussian decay to 1/*e* at 5.4 nm. *e* is a model of longitudinal sections with a mixture of cross-bridges that have either triangular shape or uniform thin width, and an angle of either 65°, 79°, or 95° with respect to the filament axis. In *f*, noise was added to the original model to imitate real EM images. The shapes and angles of the cross-bridges are still very clear in the model image with noise (*f*). In *g*, the resolution of the model image was set at 7 nm (see Materials and Methods). In *h*, the same noise as used in *f* was added to *g*. Note that the overall appearance of this model is similar to the real micrographs. *i* is a low-pass filtered image from *h*. The low-pass filter function used has a value 1.0 out to 7 nm, then falls as a Gaussian decay to 1/*e* at 6.5 nm. The blurred model images were calculated also at poorer resolution (10 nm). *j*, *k*, and *l* are the results corresponding to *g*, *h*, and *i*, but with 10-nm resolution. The low-pass filter function used for calculating *l* has a value 1.0 out to 9.5 nm, and falls as a Gaussian decay to 1/*e* at 9.0 nm.

Pollard et al. (21)). Spectroscopic studies also show that in rigor the cross-bridges attach with a fixed attachment angle, but during active ATPase activity, the heads have variable angles and are dynamically mobile (46–48).

In rigor fibers, cross-bridges adopt the periodicity of the actin filaments, although this is less striking in muscles of vertebrates than in those of invertebrates (5, 49, 50). On activation, cross-bridges shift from thin filament periodicity toward a stronger retention of the thick filament spacing (14, 15), as confirmed here by a decrease in intensity of the actin 36-nm layer line. The increase in intensity of the 43-nm layer line relative to rigor may be attributed to a greater contribution by cross-bridge mass along the thick filament helix.

In addition to the increase in intensity on the 43-nm layer line, we also observed the appearance of a layer line at 38 nm. These results suggest that in contraction the cross-bridges adopt periodicities defined by both the thick and thin filaments. In rigor the mass of the actin binding region of both heads of the myosin are constrained to attach specifically to actin on target zones where the azimuthal orientation is dictated by the actin helix. This may explain the strong layer line indexing on the 36-nm spacing of the long-pitch actin helix. If the azimuthal orientation of myosin attached to actin during contraction is less constrained, then the region along the thin filament where attachments could occur would be extended (45). Intensity on the 36-nm layer line would be diminished and the 14.3-nm meridional intensity, derived from the thick filament, would be enhanced. We observe the former, but we cannot confirm the latter from present data.

We observed a shift in layer line position, from 36 nm with a peak far from the meridian in rigor, to 38 nm with a peak much closer to the meridian in active fibers. One possible explanation might be that the actin helical repeat increases. However, it seems unlikely that the actin filament alone accounts for this change in view of the substantial shift of the peak intensity toward the meridian (Fig. 6). A more likely explanation is that portions of the active cross-bridges take up a periodicity strongly influenced by but not exactly the same as the thin filament helix. In rigor the mass of the cross-bridges is located closer to the thin filaments and more tightly constrained by the actin periodicity. The presence of the 38-nm actin-based periodicity in active muscle provides strong evidence that the active cross-bridges attach to actin at specific locations defined by the helical structure. Tsukita and Yano (14) previously observed an ~37-nm layer line in fibers during steady contraction, but did not discuss the shift from 36 nm in rigor to 38 nm in active fibers. In x-ray diffraction patterns, it has been difficult to resolve the 43-nm from the ~37-nm layer line (51–53).

Time course of structural changes during activation

The time course of disappearance of the rigor configuration and development of the features of the actively force-generating cross-bridges are represented in the micrographs of fibers frozen 20, 50, 80, and 300 ms after release of ATP

from caged ATP. Based on the tension records (Fig. 7), on the known kinetics of ATP liberation from caged ATP ($\sim 100\ s^{-1}$ (28)), and on the rates of cross-bridge detachment and reattachment in rabbit fibers (22, 31), we would expect that at the 20-ms time point, a small number of cross-bridges remain in the rigor configuration; most are not yet actively generating force. Between 50 and 300 ms there is an increase in force due to an increased number of cross-bridges actively generating tension.

At the 20-ms time point we observe cross-bridges in rigor-like configurations mixed with another population of cross-bridges with structures similar to fully active ones. These populations are distinguished by the triangular shape and tilt toward the Z-line of the rigor-like cross-bridges (15). There are few, if any, rigor-like cross-bridges in fibers frozen 50 or 300 ms after photolysis. There are several possible explanations for this finding. One is that the active cross-bridge takes a rigor configuration for a very short portion of the cycle, so that cross-bridges in this configuration represent a very small proportion of the population (22). Another possibility is that rigor cross-bridges are double-headed, while active ones are single-headed (48, 54, 55), which would result in a different appearance even if an individual active head has the other attributes of the rigor cross-bridge, e. g., attachment to a narrower target zone and tilt toward the Z-line. Finally, it is possible that the configuration of the rigor cross-bridge is never achieved by an actively cycling cross-bridge. An attached myosin head at the end of a cycle might have a shape different from that of a rigor head. In any case our results indicate that the predominant cross-bridge states populated during active force generation are very different from rigor cross-bridges, which are surprisingly rare.

A second unexpected result is the general similarity in the populations of cross-bridge configurations at 50 and 300 ms, although force approximately doubles over this interval. On the basis of the arguments presented earlier, we believe the structural preservation in our samples is sufficient to have detected major structural differences if they had been present. Mechanical and x-ray diffraction data indicate a 10–15-ms delay between cross-bridge attachment and the onset of tension (56–58) suggesting that a 10–15-ms reaction step follows attachment. This is an appreciable delay on the time scale of tension development in our experiments, and thus we expected to observe separate populations of attached cross-bridges before and during generation of tension. There are several possible explanations for the similarity of distributions of cross-bridge shapes at 50 and at 300 ms following photolysis: 1) the pre-tension state is of short duration, and thus that state is poorly populated. This possibility would require an alternative explanation for the onset of stiffness and x-ray intensity changes prior to tension mentioned above; 2) alternatively, the tension generating state is of short duration and poorly populated; 3) the structural differences between the two states are subtle, i. e., less than the variability between cross-bridges due to the periodicity mismatch between the two sets of filaments and thermal motions. If this is the case, it is puzzling how a small structural change can slide the filaments 14 nm or more. 4) At 50 ms virtually all cross-bridges might already be in the steady distribution of actively tension generating states. Since mechanical compliance at the ends of the fiber allows some sarcomere shortening, the further tension development after 50 ms might then correspond to additional power strokes and filament sliding. This further tension development might occur without a change in the overall distribution of cross-bridge configurations. However, tension development during the first 300 ms is accompanied by splitting of only approximately one ATP molecule/cross-bridge (59), so this hypothesis would suggest that cross-bridges can interact with several actin monomers for each ATP molecule used (60).

We thank D. Appelt for expert assistance and discussions in development of the freezing system, Dr. T. Reese for advice on rapid freezing experiments, Dr. H. Higuchi for helpful discussions, M. Bell and J. Pili for expert electronic and mechanical construction, X. Sun and N. Glaser for technical assistance, and Dr. H. Takekura for help in preparing figures.
Supported by an National Institutes of Health grant to the Pennsylvania Muscle Institute, a National Science Foundation grant (to J. M. Murray), and by fellowships from the Naito Foundation and the MDA (to K. Hirose).

REFERENCES

1. Reedy, M. K., K. C. Holmes, and R. T. Tregear. 1965. Induced changes in orientation of the cross-bridges of glycerinated insect flight muscle. *Nature (Lond.).* 207:1276–1280.
2. Huxley, H. E. 1969. The mechanism of muscular contraction. *Science (Washington D.C.).* 164:1356–1366.
3. Reedy, M. K. 1968. Ultrastructure of insect flight muscle. I. Screw sense and structural grouping in the rigor cross-bridge lattice. *J. Mol. Biol.* 31:155–176.
4. Heuser, J. E. 1983. Structure of the myosin crossbridge lattice in insect flight muscle. *J. Mol. Biol.* 169:123–154.
5. Varriano-Marston, E., C. Franzini-Armstrong, and J. C. Haselgrove. 1984. The structure and disposition of crossbridges in deep-etched fish muscle. *J. Muscle Res. Cell Motil.* 5:363–386.
6. Lymn, R. W., and E. W. Taylor. 1971. Mechanism of adenosine triphosphate hydrolysis by actomyosin. *Biochemistry.* 10:4617–4624.
7. Moore, P. B., H. E. Huxley, and D. J. DeRosier. 1970. Three-dimensional reconstruction of F-actin, thin filaments and decorated thin filaments. *J. Mol. Biol.* 50:279–295.
8. Taylor, K. A., and L. A. Amos. 1981. A new model for the geometry of the binding of myosin crossbridges to muscle thin filaments. *J. Mol. Biol.* 147:297–324.
9. Toyoshima, C., and T. Wakabayashi. 1985. Three-dimensional image analysis of the complex of thin filaments and myosin molecules from skeletal muscle. IV. Reconstitution from minimal- and high-dose images of the actin-tropomyosin-myosin subfragment-1 complex. *J. Biochem.* 97:219–243.
10. Milligan, R. A., and P. F. Flicker. 1987. Structural relationships of actin, myosin, and tropomyosin revealed by cryo-electron microscopy. *J. Cell Biol.* 105:29–39.
11. Milligan, R. A., M. Whittaker, and D. Safer. 1990. Molecular structure of F-actin and location of surface binding sites. *Nature (Lond.).* 348: 217–221.
12. Reedy, M. C., M. K. Reedy, and R. S. Goody. 1987. The structure of insect flight muscle in the presence of AMP-PNP. *J. Muscle Res. Cell Motil.* 8:473–503.
13. Padrón, R., and H. E. Huxley. 1984. The effect of the ATP analogue AMP-PNP on the structure of crossbridges in vertebrate skeletal muscles: X-ray diffraction and mechanical studies. *J. Muscle Res. Cell Motil.* 5:613–655.
14. Tsukita, S., and M. Yano. 1985. Actomyosin structure in contracting muscle detected by rapid freezing. *Nature (Lond.).* 317:182–184.

15. Hirose, K., and T. Wakabayashi. 1991. Conformations of crossbridges in contracting skeletal muscle. *Adv. Biophys.* 27:197–203.
16. Hirose, K., and T. Wakabayashi. 1993. Structural change of crossbridges of rabbit skeletal muscle during isometric contraction: *J. Muscle Res. Cell Motil.* In press.
17. Craig, R., L. E. Greene, and E. Eisenberg. 1985. Structure of the actin-myosin complex in the presence of ATP. *Proc. Natl. Acad. Sci. USA.* 82:3247–3251.
18. Applegate, D., and P. Flicker. 1987. New states of actomyosin. *J. Biol. Chem.* 262:6856–6863.
19. Katayama, E. 1989. The effects of various nucleotides on the structure of actin-attached myosin subfragment-1 studied by quick-freeze deep-etch electron microscopy. *J. Biochem. (Tokyo).* 106:751–770.
20. Frado, L.-L., and R. Craig. 1992. Electron microscopy of the actin-myosin head complex in the presence of ATP. *J. Mol. Biol.* 223:391–397.
21. Pollard, T. D., D. Bhandari, P. Maupin, D. Wachsstock, A. G. Weeds, and H. G. Zot. 1993. Direct visualization by electron microscopy of the weakly-bound intermediates in the actomyosin adenosine triphosphatase. *Biophys. J.* 64:454–471.
22. Goldman, Y. E., M. G. Hibberd, and D. R. Trentham. 1984. Initiation of active contraction by photogeneration of adenosine-5′-triphosphate in rabbit psoas muscle fibres. *J. Physiol. (Lond.).* 354:605–624.
23. Hirose, K., T. D. Lenart, C. Franzini-Armstrong, and Y. E. Goldman. 1991. Flash and smash: ultrastructure of rabbit muscle fibers rapidly frozen following photolysis of caged ATP. *Biophys. J.* 59:577*a*. (Abstr.)
24. Hirose, K., J. M. Murray, C. Franzini-Armstrong, and Y. E. Goldman. 1991. Flash and smash: conformational changes of muscle fibers rapidly frozen following photolysis of caged ATP. *J. Cell Biol.* 115:334*a*. (Abstr.)
25. Heuser, J. E., T. S. Reese, M. J. Dennis, Y. Jan, L. Jan, and L. Evans. 1979. Synaptic vesicle exocytosis captured by quick freezing and correlated with quantal transmitter release. *J. Cell Biol.* 81:275–300.
26. Padrón, R., L. Alamo, R. Craig, and C. Caputo. 1988. A method for quick-freezing live muscles at known instants during contraction with simultaneous recording of mechanical tension. *J. Microsc. (Oxf.).* 151: 81–102.
27. Goldman, Y. E., and R. M. Simmons. 1984. Control of sarcomere length in skinned muscle fibres of *Rana temporaria* during mechanical transients. *J. Physiol. (Lond.).* 350:497–518.
28. Goldman, Y. E., M. G. Hibberd, and D. R. Trentham. 1984. Relaxation of rabbit psoas muscle fibres from rigor by photochemical generation of adenosine-5′-triphosphate. *J. Physiol. (Lond.).* 354:577–604.
29. Ward, R., and J. M. Murray. 1987. Natural propane cryogen for frozen-hydrated biological specimens. *J. Electron Microsc. Tech.* 5:275–277.
30. Henderson, R., J. M. Baldwin, K. H. Downing, J. Lepáult, and F. Zemlin. 1986. Structure of purple membrane from *Halobacterium halobium*: recording, measurement and evaluation of electron micrographs at 3.5 Å resolution. *Ultramicroscopy.* 19:147–178.
31. Goldman, Y. E. 1987. Kinetics of the actomyosin ATPase in muscle fibers. *Annu. Rev. Physiol.* 49:637–654.
32. Fajer, P. G., E. A. Fajer, and D. D. Thomas. 1990. Myosin heads have a broad orientational distribution during isometric muscle contraction: time-resolved EPR studies using caged ATP. *Proc. Natl. Acad. Sci. USA.* 87:5538–5542.
33. Ostap, E. M., V. A. Barnett, and D. D. Thomas. 1993. Steady-state and transient detection of spin-labeled myosin's conformational changes during ATP hydrolysis in the muscle fiber. *Biophys. J.* 64:361*a*.
34. Tanner, J. W., D. D. Thomas, and Y. E. Goldman. 1992. Transients in orientation of a fluorescent cross-bridge probe following photolysis of caged nucleotides in skeletal muscle fibres. *J. Mol. Biol.* 223:185–203.
35. Poole, K. J. V., Y. Maeda, G. Rapp, and R. S. Goody. 1991. Dynamic X-ray diffraction measurements following photolytic relaxation and activation of skinned rabbit psoas fibres. *Adv. Biophys.* 27:63–75.
36. Bridgman, P. C., and T. S. Reese. 1984. The structure of cytoplasm in directly frozen cultured cells. I. Filamentous meshworks and the cytoplasmic ground substance. *J. Cell Biol.* 99:1655–1668.
37. Craig, R., L. Alamo, and R. Padrón. 1992. Structure of the myosin filaments of relaxed and rigor vertebrate striated muscle studied by rapid freezing electron microscopy. *J. Mol. Biol.* 228:474–487.
38. Lepault, J., I. Erk, G. Nicolas, and J.-L. Ranck. 1991. Time-resolved cryo-electron microscopy of vitrified muscular components. *J. Microsc. (Oxf.).* 161:47–57.
39. Lenart, T. D., T. StC. Allen, R. J. Barsotti, G. C. R. Ellis-Davies, J. H. Kaplan, C. Franzini-Armstrong, and Y. E. Goldman. 1992. Mechanics and structure of cross-bridges during contractions initiated by photolysis of caged Ca^{2+}. *In* Mechanism of Myofilament Sliding in Muscle Contraction. H. Sugi, editor. Plenum Press, New York. 475–486.
40. Bard, F., C. Franzini-Armstrong, and W. Ip. 1987. Rigor crossbridges are double-headed in fast muscle from crayfish. *J. Cell Biol.* 105:2225–2234.
41. Irving, M., V. Lombardi, G. Piazzesi, and M. A. Ferenczi. 1992. Myosin head movements are synchronous with the elementary force-generating process in muscle. *Nature (Lond.).* 357:156–158.
42. Murray, J. M., T. D. Lenart, C. Franzini-Armstrong, and Y. E. Goldman. 1993. Structural changes in cross-bridges of skinned muscle fibers activated by photolysis of caged Ca^{2+} and rapidly frozen for electron microscopy. *Biophys. J.* 64:26*a*. (Abstr.)
43. Huxley, H. E., and W. Brown. 1967. The low-angle X-ray diagram of vertebrate striated muscle and its behaviour during contraction and rigor. *J. Mol. Biol.* 30:383–434.
44. Haselgrove, J. C. 1975. X-ray evidence for conformational changes in the myosin filaments of vertebrate striated muscle. *J. Mol. Biol.*3 92: 113–143.
45. Haselgrove, J. C., and M. K. Reedy. 1978. Modeling rigor cross-bridge patterns in muscle. I. Initial studies of the rigor lattice of insect flight muscle. *Biophys. J.* 24:713–728.
46. Cooke, R., M. S. Crowder, and D. D. Thomas. 1982. Orientation of spin labels attached to cross-bridges in contracting muscle fibres. *Nature (Lond.).* 300:776–778.
47. Berger, C. L., E. C. Svensson, and D. D. Thomas. 1989. Photolysis of a photolabile precursor of ATP (caged ATP) induces microsecond rotational motions of myosin heads bound to actin. *Proc. Natl. Acad. Sci. USA.* 86:8753–8757.
48. Stein, R. A., R. D. Ludescher, P. S. Dahlberg, P. G. Fajer, R. L. H. Bennett, and D. D. Thomas. 1990. Time-resolved rotational dynamics of phosphorescent-labeled myosin heads in contracting muscle fibers. *Biochemistry.* 29:10023–10031
49. Reedy, M. K., and M. C. Reedy. 1985. Rigor crossbridge structure in tilted single filament layers and flared-X formations from insect flight muscle. *J. Mol. Biol.* 185:145–176.
50. Taylor, K. A., M. C. Reedy, L. Córdova, and M. K. Reedy. 1989. Three-dimensional image reconstruction of insect flight muscle. I. The rigor myac layer. *J. Cell Biol.* 109:1085–1102.
51. Yagi, N. 1991. Intensification of the first actin layer-line during contraction of frog skeletal muscle. *Adv. Biophys.* 27:35–43.
52. Bordas, J., G. P. Diakun, J. E. Harries, R. A. Lewis, G. R. Mant, M. L. Martin-Fernandez, and E. Towns-Andrews. 1991. Two-dimensional time resolved X-ray diffraction of muscle: recent results. *Adv. Biophys.* 27:15–33.
53. Wakabayashi, K., H. Tanaka, H. Saito, N. Moriwaki, Y. Ueno, and Y. Amemiya. 1991. Dynamic X-ray diffraction of skeletal muscle contraction: structural change of actin filaments. *Adv. Biophys.* 27:3–13.
54. Fajer, P. G., E. A. Fajer, N. J. Brunsvold, and D. D. Thomas. 1988. Effects of AMP-PNP on the orientation and rotational dynamics of spin-labeled myosin heads in muscle fibers. *Biophys. J.* 53:513–524.
55. Berger, C. L., and D. D. Thomas. 1993. Rotational dynamics of actin-bound myosin heads in active myofibrils. *Biochemistry.* 32:3812–3821.
56. Ford, L. E., A. F. Huxley, and R. M. Simmons. 1986. Tension transients during the rise of tetanic tension in frog muscle fibres. *J. Physiol. (Lond.).* 372:595–609.
57. Kress, M., H. E. Huxley, A. R. Faruqi, and J. Hendrix. 1986. Structural changes during activation of frog muscle studied by time-resolved X-ray diffraction. *J. Mol. Biol.* 188:325–342.
58. Barsotti, R. J., G. Ellis-Davies, J. H. Kaplan, and Y. E. Goldman. 1989. Kinetics of skeletal muscle fiber activation by photolysis of DM-nitrophen (caged Ca^{2+}) and caged ATP. *Biophys. J.* 55:10*a*. (Abstr.)
59. Ferenczi, M. A., E. Homsher, and D. R. Trentham. 1984. The kinetics of magnesium adenosine triphosphate cleavage in skinned muscle fibres of the rabbit. *J. Physiol.* 352:575–599.
60. Harada, Y., K. Sakurada, T. Aoki, D. D. Thomas, and T. Yanagida. 1990. Mechanochemical coupling in actomyosin energy transduction studied by in vitro movement assay. *J. Mol. Biol.* 216:49–68.